

An Ab Initio Study on the Structural, Electronic and Optical Properties of Inverted Sandwich Monocyclic Small Boron Clusters Zn_nB_m ($n=1, 2$; $m=6-8$)

Maliha Nishat¹, Md Kamal Hossain², Md. Rakib Hossain³, Milon Milon⁴, Farid Ahmed², Tahmina Ferdous², and Md. Abul Hossain²

¹Pabna University of Science and Technology

²Jahangirnagar University

³Bangabandhu Sheikh Mujibur Rahman Science and Technology University

⁴Comilla University

July 6, 2020

Abstract

For the past decades, experiment like photoelectron spectroscopy and computational studies have demonstrated that highly coordinated transition metal centered boron nanoclusters favor planar or quasi-planar type structures, which could be potential building blocks for designing better nanostructure with tailored properties. In this paper, we have studied geometrical structures, electronic, optical and magnetic properties of the gas-phase Zn centered small boron clusters ($n = 6-8$) by employing density functional theory (DFT) and time dependent (TD) DFT calculations with B3LYP hybrid exchange-correlation functional. Two global minimum structures containing pyramidal and bi-pyramidal shaped ZnB_m and Zn_2B_m clusters shows symmetrical cyclic motif. The adsorption energy, ionization potential and molecular orbital analysis revealed that Zn is chemically adsorbed on the boron clusters occupying the hollow site and inverse sandwich bi-pyramidal (Zn_2B_m) clusters are relatively more stable compared to singly doped boron nanoclusters. Vibrational modes are calculated to validate the true minima nature of the optimize structures which possesses no imaginary frequencies. All the pyramidal and bi-pyramidal clusters are optically active and show blue shifts in our calculated absorption spectra. The DFT computations indicate spin polarization in the pristine B7 cluster which induces strong ferromagnetism in pristine and adsorbed B7 clusters.

Keywords

Boron nanoclusters, inverse sandwich molecules, DFT, structural stability, adsorption energy.

Introduction

In recent times, the study of atomic and molecular cluster has drawn more attention as these clusters provides a link between bulk and nanostructured materials [1]. Earlier in 1956, Becker first reported the experimental method of producing a large variety of neutral and ionized clusters such as LaB_6 [2]. Till now, many clusters have been investigated theoretically and also by experiments like photoelectron spectroscopy [3]. As an electron-deficient semimetal, Boron (B) has high electronegativity, large co-ordination number, short covalent radius and possesses attractive physical properties [4]. Because of these phenomenon, boron emerges as a favorable candidate in device section which include variety of sectors from medicine to hydrogen

storage industry [5–8]. As a result, boron clusters (B_m) have gained a considerable interest of the researchers. At first Boustani computationally explored the geometric structures of B_m ($m \leq 14$) clusters by employing Hartree-Fock method in restricted mode and quasiplanar structures of boron were predicted to be more stable form in case of small clusters [9–11]. Later these result were reaffirmed by Wang *et al.* [12, 13] who performed both theoretical and experimental investigation. Anderson *et al.* carried an experimental study on the mass spectra of boron clusters where these clusters were produced in easiest way like the laser ablation technique [14]. The early theoretical investigation were performed for neutral and anionic B_3 – B_{15} clusters [13, 15–20] and confirmed the planar or quasiplanar type atomic arrangements of these clusters.

Doping of various atom on boron clusters opens up the possibility of unique boron based nanostructures which contains some intriguing properties [21]. There are many investigations on transition metal doped pyramidal B_m nanoclusters [3, 22–25] which concerns about the stability and bonding mechanism of the clusters. Moreover, transition-metal (TM) dopants (Cr, Mn, Fe, Co, Ni, Zr) can interestingly change the geometry of small boron based nanoclusters [26–28]. Recently, transition metal (TM) appears as an interesting dopant in boron nanoclusters in both theoretical and experimental sectors. These type of TM doped clusters are very fascinating as they offer a building blocks to explore new molecular and nanostructures with novel chemical and physical phenomenon [3, 24, 27, 29–31]. A theoretical investigation by DFT calculations have been performed with TM at the center of a double-ring boron clusters $M@B_{2n}$ ($M = Ti, Cr, Fe, Ni, Zn; n = 6, 7, 8$) and found double aromaticity in those clusers [32]. Bi-pyramidal boron nanoclusters are not much focused in contrast to pyramidal boron cluster [33–36]. A combined theoretical and experimental investigation was carried on Ta_2B_6 to analyze their chemical bonding and found that bi-pyramidal structures are one of the stable with D_{6h} symmetry [37]. The optical excitation nature of small boron nanoclusters ($n = 2-5, 6, 12$ and 13) have been reported and found the collective and plasmonic behavior of the electronic excitations in most of them [38]. Magnetic properties are less explored and in one of the study it was found that the magnetic properties mainly come from the boron atoms and the overall magnetic moments are very specific with the number of boron atoms [23]. The inverted sandwich structures with two TM atoms sandwiching the central cyclic molecule exhibits fascinating chemical, opto-electronic and magnetic properties [39]. Many experiments and computational studies have suggested that the inverted sandwich small boron complexes are more stable configuration [40]. More study should be conducted to understand the stability of such boron clusters which have inverse-sandwich structures and their properties. In this regard a small investigation has done on B_6 by adsorbing Zn atom by the author of this article where Zn_2B_6 show metallic behavior [41]. This motivates to perform detailed investigation of Zn adsorbed boron nanoclusters. Furthermore, there were few works regarding Zn doped nanoclusters and their inverted-sandwich structures with pyramidal and bipyramidal shape, though it shows better properties as dopant and can be used in sensing applications and future phototherapy applications for carbon dots. and etc. [42–44].

In this article, we report an investigation on the geometry, stability, electronic, magnetic and optical properties of pristine and Zn adsorbed inverted sandwich boron nanoclusters, Zn_nB_m ($m=6-8$) with pyramidal and bi-pyramidal shapes. This work has been carried out under density functional theory (DFT). To understand structural stability, the adsorption energies (E_{Ads}), cohesive energies (E_{Coh}), thermodynamical parameters, lowest vibrational energies of the clusters have been investigated. The global indices such as chemical potential, chemical hardness, electrophilicity, chemical softness have been calculated from highest occupied molecular orbital (HOMO) and lowest unoccupied molecular orbital (LUMO) energies for observing the chemical reactivity. The HOMO-LUMO gaps, Mulliken charge exploration and dipole moment have further been studied to analyze the electronic nature of these nanoclusters. We have studied magnetic behaviors of the clusters by calculating magnetic moment and spin density map. The optical properties have been studied from the calculated absorption spectra and circular dichroism (CD) spectra which describe the interaction of electromagnetic radiation with pristine and Zn adsorbed B_m nanoclusters and optical activity respectively.

Computational Details

In this work we have employed density functional theory (DFT) that is implanted in Gaussian 16 package with B3LYP as hybrid functional [45–47]. Since investigating clusters contain very few number of atoms (from 6 to 10) and the atomic number of constituent atoms (B and Zn) is 5 and 30 respectively, we have taken LanL2DZ basis set which is suitable for the system containing the element H(1) to Bi (83) [48]. SDD basis set has also employed to compare the results which is applicable for the system containing the element H(1) to Hg (80) [49]. The B3LYP is one of the reliable and routinely implemented level of theory in various investigation of different nanoclusters [50–52]. Initially all the clusters of pristine B₆, B₇ and B₈ were fully optimized and then Zn atom was absorbed in pyramidal and bi-pyramidal fashion in these clusters. The adsorbed clusters which are inverse-sandwich shape again relaxed to global minima by using the same basis sets. All calculations are done in spin unrestricted conditions to determine the magnetic properties (magnetic moment and spin density map) of these clusters. The lowest vibrational frequency and the number of imaginary frequency have investigated from vibrational frequency analysis. For investigating electrical and optical properties, the excited states of these clusters have been calculated by using TD-DFT approach.

To understand the relative stability of these clusters we have calculated adsorption energy (E_{Ads}) and cohesive energy per atom (E_{Coh}). The adsorption energy of the adsorbed clusters can be calculated by the equations [53]-

$$E_{\text{Ads}} = E_{\text{Zn}_i\text{B}_m} - (E_{\text{B}_m} + iE_{\text{Zn}}) \quad (1)$$

The cohesive energy per atom can be calculated as [53]:

$$E_{\text{Coh}} = \frac{E_{\text{Zn}_i\text{B}_m} - (mE_{\text{B}} + iE_{\text{Zn}})}{m+i} \quad (2)$$

here the symbol i ($=1, 2$) denotes the number of Zn atom and m ($=6-8$) represents the number of boron atom. $E_{\text{Zn}_i\text{B}_m}$, E_{B_m} and E_{Zn} represent the total energy of Zn doped B _{m} cluster, the energy of B _{m} motif and the energy of a single Zn atom respectively. For better insight of the adsorption phenomena, we have further analyzed the thermodynamic properties which include the changes of Gibbs free energy (ΔG), enthalpy (ΔH) and entropy (ΔS) by the following equations [54]:

$$G = G_{\text{Zn}_i\text{B}_m} - (iG_{\text{Zn}} + G_{\text{B}_m}) \quad (3)$$

$$H = H_{\text{Zn}_i\text{B}_m} - (iH_{\text{Zn}} + H_{\text{B}_m}) \quad (4)$$

$$S = \frac{H-G}{T} \quad (5)$$

here G stands for the sum of electronic and thermal free energies, H refers to the sum of electronic and thermal free enthalpies and T represents the standard room temperature (298.15 K) of optimized geometries. The charge transfers between the pristine and Zn adsorbed B _{m} nanoclusters have been investigated by Mulliken charge analysis and molecular electrostatic potential (MEP) map. The HOMO and LUMO energies are computed for calculating the energy gap (E_g), Fermi level energy (E_{FL}) and density of states (DOS) plots,

$$E_g = E_{\text{LUMO}} - E_{\text{HOMO}} \quad (6)$$

$$E_{\text{FL}} = \frac{E_{\text{HOMO}} + E_{\text{LUMO}}}{2} \quad (7)$$

The chemical potential (μ), global indices such as hardness (η), softness (S), electrophilicity (ω) and charge transfer parameters ($[?]N$) of the adsorption systems are calculated as [55]-

$$\mu = \frac{-(IP+EA)}{2} \quad (8)$$

$$\eta = \frac{(IP-EA)}{2} \quad (9)$$

$$S = \frac{1}{2\eta} \quad (10)$$

$$\omega = \frac{\mu^2}{2\eta} \quad (11)$$

$$N = -\frac{\mu}{\eta} \quad (12)$$

where $IP = -E_{\text{HOMO}}$ and $EA = -E_{\text{LUMO}}$ are the ionization potential and electron affinity respectively [56, 57]. Optical properties have also investigated by using absorption spectra and CD spectra with B3LYP/SDD density functional level of theory.

Results and Discussions

Structural Properties

Geometry of the global minimum structures

We have presented our results by exhibiting the optimized geometries of pristine and Zn incorporated inverse-sandwich boron nanoclusters in Fig. 1. Pristine B_6 structure has a cyclic benzene like planar structure with C_{2h} symmetry which is predicted to be the global minimum structure [58–60]. Symmetry changes to C_1 for pyramidal and bi-pyramidal B_6 structures [61] as shown in Table 1 for two basis sets. These global minimum structures also shows planer shapes that have observed in Fig. 1. The symmetrical bond length of B_6 between the nearest neighbors is 1.547 Å, obtained by an angle of 135.69° except for B2-B3 and B5-B6 which are 1.632 Å. For the adsorbed B_6 systems, bond lengths are slightly changes to maintain the equilibrium which has presented in supplementary material (Table S1). The lowest frequency of the pristine B_6 is 309.68 cm^{-1} for SDD basis set (311.30 cm^{-1} for LanL2DZ) which is displayed in Table 1. But there exists one imaginary frequency in pristine B_6 for both basis sets [59]. While for the inverse-sandwich B_6 structures the value of lowest frequency decreases and no imaginary frequency is observed at the B3LYP/SDD and B3LYP/LanL2DZ level of theory. Pristine B_7 cluster has slightly distorted cyclic heptagonal shape with lowest energy structures of C_s symmetry [58, 62]. Again for the adsorbed B_7 clusters, symmetry changes to C_1 [61] as does the bond lengths and the structures show almost planer shape except for ZnB_7 . In ZnB_7 , two atoms (B5 and B6) are out of the plane as shown in Fig. 1. The average peripheral B–B bond length of pristine B_7 is about 1.584 Å and it is very close to the experimental B–B bond length of B_2 (1.59 Å) [63]. No imaginary frequency is observed for all the B_7 clusters except Zn_2B_7 for LanL2DZ basis set.

For B_8 , an aromatic octagon with D_{4d} symmetry (in Table 1) is the lowest-energy structure [58] and again symmetry changes to C_1 for the dopant atom (Zn) on B_8 ring in pyramidal and bi-pyramidal fashion for both basis sets. The overall bond lengths of all B-B are 1.565 Å in pristine B_8 and for the adsorbed clusters bond lengths are slightly increases (on average 1.582 Å) in both basis sets. This reveals that cyclic boron rings are favorable for adsorbing metal atoms which causes the enhancement of bond length. All the B_8 clusters are planar shape as shown in Fig. 1 except for ZnB_8 where three atoms (B4, B5 and B6) are out of plane. We have found no imaginary frequency for all the B_8 clusters (in both SDD and LanL2DZ). The value of the lowest frequency increases like $B_8 > ZnB_8 > Zn_2B_8$ and this reveals that our inverse-sandwich clusters are more stable. Further in two basis sets (SDD and LanL2DZ), bond lengths and bond angles doesn't vary that much for all the pristine and inverse-sandwich B_m nanoclusters. All B_7 clusters possesses ground-state spin multiplicity in doublet state [9], while singlet for all B_6 and B_8 clusters.

Relative Stability

The relative stabilities can be analyzed by calculating different parameters like adsorption energy (E_{Ads}) and cohesive energy (E_{Coh}) per atom using equation (1 and 2) which are listed in Table 2.

Hosted file

image1.emf available at <https://authorea.com/users/302041/articles/463473-an-ab-initio-study-on-the-structural-electronic-and-optical-properties-of-inverted-sandwich-monocyclic-small-boron-clusters-znbn-n-1-2-m-6-8>

Fig. 1 Optimized structural configuration for adsorbing Zn on B_m ($m=6-8$) nanoclusters in inverse-sandwich shape (arrow represent nearest and next nearest in-plane atoms from origin point).

Table 1 Data of lowest infrared absorptions, dipole moment μ_D and point group for pristine as well as Zn adatom on B_m ($m=6-8$) nanoclusters.

System	Lowest Frequency (cm^{-1})	Lowest Frequency (cm^{-1})	No. of Imaginary Frequency	No. of Imaginary Frequency	μ_Δ (Debye)	μ_Δ (Debye)	Point Group	Point Group
B_6	SDD 309.68	LanL2DZ 311.30	SDD 1	LanL2DZ 1	SDD 0	LanL2DZ 0	SDD C_{2H}	LanL2DZ C_{2H}
ZnB_6	180.23	87.74	0	0	3.567	4.703	C_1	C_1
Zn_2B_6	153.84	214.25	0	0	0	0	C_1	C_1
B_7	121.47	121.89	0	0	0.175	0.174	C_S	C_S
ZnB_7	41.12	53.00	0	0	3.170	4.228	C_1	C_1
Zn_2B_7	31.93	187.52	0	1	0.027	0.035	C_1	C_1
B_8	51.69	62.48	0	0	0	0	D_{4D}	D_{4D}
ZnB_8	85.06	117.77	0	0	2.167	3.217	C_1	C_1
Zn_2B_8	166.38	181.92	0	0	0.009	0.0002	C_1	C_1

Adsorption energy defines the energy difference between the total energies of individual constituent atoms and the bound cluster and the more negative values of adsorption energies indicate the more tightly bound system [64]. The variation of adsorption energy has shown in Fig. 2(a) for adsorbed boron nanoclusters and here observe that E_{Ads} increases for bi-pyramidal structures for all the boron nanoclusters. Also these values are increases with the increase of the cluster size of boron [58]. This phenomenon also occurs because one atom participates in the charge transfer process for pyramidal B_m whereas two Zn atom participates in bi-pyramidal and so the value of E_{Ads} are increased. Thus, the doubly doped pyramidal boron cluster stabilizes the nanostructures and Zn_2B_m clusters are more stable. This implies that as soon as a cluster gains extra electron in bi-pyramidal fashion, it becomes more stable than its pyramidal structure.

Table 2 Ground state energy, Adsorption energy (E_{Ads}) in eV unit and Cohesive Energy (E_{Coh}) per atom in eV/atom unit of pure as well as Zn adsorbed B_m ($m= 2-6$) nanoclusters for two basis set.

System	Ground state energy	Ground state energy	E_{Ads}	E_{Ads}	E_{Coh}	E_{Coh}
B_6	SDD -4046.	LanL 2DZ -4046	SDD -	LanL 2DZ -	SDD -3.37	LanL 2DZ -3.37
ZnB_6	-10228	-5831	-6.35	-5.59	-3.79	-3.79
Zn_2B_6	-16408	-7616	-11.75	-10.59	-3.99	-3.99
B_7	-4723	-4723	-	-	-3.69	-3.69
ZnB_7	-10904	-6508	-6.45	-5.65	-4.03	-4.03
Zn_2B_7	-17086	-8294	-13.06	-11.77	-4.32	-4.32
B_8	-5397	-5397	-	-	-3.60	-3.60
ZnB_8	-11581	-7184	-8.64	-7.78	-4.16	-4.16
Zn_2B_8	-17764	-8971	-16.27	-15.06	-4.51	-4.51

Hosted file

image2.emf available at <https://authorea.com/users/302041/articles/463473-an-ab-initio-study-on-the-structural-electronic-and-optical-properties-of-inverted-sandwich-monocyclic-small-boron-clusters-znbnm-n-1-2-m-6-8>

Fig. 2 Variations of (a) Adsorption energy (E_{Ads}) and Cohesive Energy (E_{Coh}) per atom in eV for Zn adsorbed boron nanoclusters.

Cohesive energy is defined as the amount of energy to break something up into single atoms. The energetic stability of the systems [65] is specified by the values of E_{coh} and the lesser the E_{coh} value, the more stable the system is [66]. The variation of E_{coh} for the adsorbed clusters has shown in Fig. 2(b). The obtained negative values of cohesive energies presented in Table 2 indicate that all the pristine and adsorbed boron nanoclusters are energetically stable. It was also observed (Fig. 2(b)) that the cohesive energy decreases with the increase of the size of inverse-sandwich boron nanoclusters which shows that energetic stability increases with the increase of the no. of adatom on B_m nanoclusters. Bi-pyramidal systems give the lowest cohesive energy was and found highest value for the pristine B_m . These results show that Zn_2B_m clusters are more stable than the other clusters which are a reaffirmation of our investigation.

Thermodynamic Parameters

Thermodynamic properties give better insight to the adsorption behavior of Zn on B_m structure. The thermodynamic properties which include change of Gibbs free energy (ΔG), enthalpy (ΔH) and entropy (ΔS) have calculated by using equation (3-5) and listed them in Table 3. For adsorbed clusters, variation of ΔH and ΔG are displayed in Fig. 3. Enthalpy (ΔH) is used as an indicator for classifying the adsorption process (Either chemisorption or physisorption). If the value of ΔH is less than 0.42eV (40KJmol^{-1}) or greater than 0.83eV (80KJmol^{-1}) then it either indicates physisorption or implies strong chemisorption respectively [67].

Hosted file

image3.emf available at <https://authorea.com/users/302041/articles/463473-an-ab-initio-study-on-the-structural-electronic-and-optical-properties-of-inverted-sandwich-monocyclic-small-boron-clusters-znbnm-n-1-2-m-6-8>

Fig. 3 Illustration of various thermodynamic properties (changes of (a) Enthalpy and (b) Gibbs free energy) for pyramidal and bi-pyramidal B_m nanoclusters where $m=6-8$.

In this study, the adsorption is chemisorption (ΔH ranges from 0.465 to 4.295) for all adsorbed B_m nanoclusters except the pyramidal and bi-pyramidal B_6 clusters where physisorption occurs in two basis sets. Besides, positive and negative signs have noted for the value of ΔH for inverse-sandwich clusters that points to endothermic and exothermic nature respectively.

The negative change of entropy (ΔS) points the ordered adsorptions [54]. The negative value of Gibbs free energy (ΔG) indicates the probability of the process and spontaneous nature of the adsorption [67] and here all the adsorbed clusters except ZnB_6 exhibits it. Also, with the increase of the size of the adsorbed B_m clusters, the value of ΔH and ΔG increases and it corresponds to the thermodynamic stability of the inverted sandwich bi-pyramidal clusters except Zn_2B_6 .

Table 3 List of thermodynamic properties (Changes of enthalpy (ΔH), Gibbs free energy (ΔG) in electronVolt (eV) unit, Entropy (ΔS) in electronVolt/mole.Kelvin (eV/Mole.K) unit) for Zn adsorbed inverse-sandwich boron nanoclusters by using two basis set.

System	ΔH	ΔH	ΔG	ΔG	ΔS	ΔS
	SDD	LanL 2DZ	SDD	LanL 2DZ	SDD	LanL 2DZ
ZnB_6	-0.37	-0.21	-0.05	0.08	-0.001	-0.001
Zn_2B_6	0.20	0.43	0.95	1.20	-0.002	-0.003

System	ΔH	ΔH	$\Delta \Gamma$	$\Delta \Gamma$	$\Delta \Sigma$	$\Delta \Sigma$
ZnB ₇	-0.47	-0.26	-0.09	0.11	-0.001	-0.001
Zn ₂ B ₇	-1.11	-1.05	-0.31	-0.19	-0.003	-0.003
ZnB ₈	-2.65	-2.39	-2.20	-1.96	-0.002	-0.001
Zn ₂ B ₈	-4.30	-4.28	-3.40	-3.39	-0.003	-0.003

Electronic Properties

Charge Distribution Analysis

Charge density distributions has a crucial character in the field of quantum chemical calculation for molecular system because it affects electronic properties of these molecular systems [68]. In this study Mulliken charge distribution and partial charge of constituent atoms have been calculated by using B3LYP level of theory and listed them in Table 4. The charge distributions of the clusters are depicted in Fig. 4. Comparing pristine and adsorbed B₆ and B₇ structures, the value of overall Q_{Mulliken} is found to be low for adsorbed clusters, while for B₈ clusters, Mulliken charge increases from its pristine clusters. From Fig. 4 we have observed that in the B₆ and B₇ structure only B1 and B4 atom are negatively charged whereas the other atoms are the electron donor which is also clearly depicted in Fig. 5(a, b) and the structure is planar. On the other hand, pristine B₈ is charge neutral and that's why no color variations are observed in Fig. 5(c). However, for inverse-sandwich B₆ clusters (pyramidal and bi-pyramidal) orbital overlapping happened for Zn atom with boron atoms and it leaves impact in the electron density which is understood by the deviation in color gradient.

Hosted file

image4.emf available at <https://authorea.com/users/302041/articles/463473-an-ab-initio-study-on-the-structural-electronic-and-optical-properties-of-inverted-sandwich-monocyclic-small-boron-clusters-znbnm-n-1-2-m-6-8>

Fig. 4 Mulliken charge distribution of pristine and Zn adsorbed B_m (m=6-8) structures in pyramidal and bi-pyramidal fashion. Here red color indicates electron acceptor and green color refers the electron donor.

Also, the negative values of charge transfer parameter ($[?]N$) for all adsorbed clusters demonstrate that the B_m clusters have an acceptor electron effect and Zn atom has a donor electron effect. As a result, we have noticed that the positive charge is localized on Zn atom and all the B atoms are negatively charged in the B₆ clusters (Fig. 5(a)). This phenomenon is arisen for the variance of electronegativity between dopant (Zn) and framework (boron atoms). As the electronegativity of boron (2.04) not very much larger than Zn (1.65), so there is a weak electrostatic attraction between them. With the increase of cluster size, Zn atom remains positively charged while boron frameworks become positively and negatively charged for all the adsorbed B₇ and B₈ clusters except Zn₂B₈. For this inverse sandwich molecule, Zn atom is negatively charged for SDD basis set and positively charged for LanL2DZ basis set. These occur due to the combined electronegativity effect of the constituent's atom of the cluster because the clusters size increases. Also, in terms of partial charges both the basis set show almost similar pattern for all the pristine and adsorbed clusters except some little variations that we already observed in Fig. 4.

Table 4 Different electrical parameters of the pristine and Zn adsorbed B_m nanoclusters.

Parameters	Basis Sets	B ₆	ZnB ₆	Zn ₂ B ₆	B ₇	ZnB ₇	Zn ₂ B ₇	B ₈	ZnB ₈	Zn ₂ B ₈
Q_{Mulliken}	SDD	0.290	0.179	0.036	0.195	0.178	0.061	0.001	0.227	0.025
	LanL2DZ	0.284	0.382	0.405	0.194	0.353	0.420	0.001	0.428	0.285
Partial charge of ad atom	SDD	-	0.179	0.036	-	0.161	0.017	-	0.114	-0.025
	LanL2DZ	-	0.382	0.405	-	0.050	0.419	-	0.292	0.285

Parameters	Basis Sets	B ₆	ZnB ₆	Zn ₂ B ₆	B ₇	ZnB ₇	Zn ₂ B ₇	B ₈	ZnB ₈	Zn ₂ B ₈
E _{HOMO} (eV)	SDD	-5.61	-5.67	-4.72	-6.63	-5.98	-5.46	-5.90	-6.02	-6.14
	LanL2DZ	-5.61	-5.46	-4.49	-6.63	-5.94	-5.23	-5.90	-6.01	-5.95
E _{LUMO} (eV)	SDD	-4.84	-3.47	-4.63	-4.62	-4.08	-4.21	-4.73	-4.87	-3.92
	LanL2DZ	-4.84	-3.35	-4.15	-4.62	-3.88	-4.17	-4.74	-4.60	-3.90
E _{FL} (eV)	SDD	-5.23	-4.57	-4.68	-5.63	-5.03	-4.84	-5.32	-5.45	-5.03
	LanL2DZ	-5.23	-4.41	-4.32	-5.63	-4.91	-4.70	-5.32	-5.31	-4.93
E _g (eV)	SDD	0.77	2.20	0.09	2.01	1.90	1.25	1.17	1.15	2.22
	LanL2DZ	0.77	2.11	0.34	2.01	2.06	1.06	1.16	1.41	2.05
[?]N (eV)	SDD	-	-4.16	-103.89	-	-5.29	-7.74	-	-9.47	-4.53

Hosted file

image5.emf available at <https://authorea.com/users/302041/articles/463473-an-ab-initio-study-on-the-structural-electronic-and-optical-properties-of-inverted-sandwich-monocyclic-small-boron-clusters-znbnm-n-1-2-m-6-8>

Fig. 5 Partial Mulliken charges of Pristine and adsorbed B_mclusters for different basis set.

The molecular electrostatic potential (MEP) map is used to define regions of electron density localization and delocalization in the interior of molecular structures [69, 70]. These maps are beneficial for identifying electrophilic or nucleophilic region of the compound and it helps to determine the charge circulation around the surface of the compound. All calculated results of pristine and Zn adsorbed boron nanoclusters are shown in Fig. 6. Here, the electrophilic and nucleophilic regions identified by the red and blue colors which also represent the negative and positive charges respectively. The observed maps indicate a positive potential in all adsorbed clusters (blue color is shown around the Zn atom), while red color, a negative potential is confined to the B_m nanoclusters.

Hosted file

image6.emf available at <https://authorea.com/users/302041/articles/463473-an-ab-initio-study-on-the-structural-electronic-and-optical-properties-of-inverted-sandwich-monocyclic-small-boron-clusters-znbnm-n-1-2-m-6-8>

Fig. 6 Molecular Electrostatic Potential (MEP) map for all pristine and adsorbed B_m nanoclusters at iso-scale value of 0.007. Regions of higher electron density are shown in red and of lower electron density in blue (values in atomic units).

These outcomes are comparable to the Mulliken charge calculations. Therefore in the adsorbed clusters, the dopant atom holds donor electron consequence. That's why charge transfer occurs slightly (the value of [?]N) between the boron nanoclusters and the Zn atom.

Dipole Moment

The dipole moment is a vital electronic property that counts the irregular charge circulation of the components of a molecule and with more dipole moment the structure becomes more polar [71]. Moreover it is a convenient pointer for knowing adsorption phenomena (adsorbate-adsorbent interaction). The dipole moment (μ_D) of pristine and Zn adsorbed B_mclusters have been calculated and listed in Table 1. Pristine and bi-pyramidal B₆ clusters have no dipole moment as they possess symmetric structure. An exception observed for ZnB₆ (3.569 for SDD and 4.703 for LanL2DZ). But unusually all the B₇ clusters show dipole moment. Pristine and pyramidal B₇ clusters are polar ($\mu_D=0.035-0.175$ D) while bi-pyramidal clusters are strongly polar ($\mu_D=3.170$ for SDD and 4.228 for LanL2DZ) [72]. Pristine B₈ have no dipole moment and bi-pyramidal B₈ is slightly polar while pyramidal ZnB₈ are strongly polar ($\mu_D=2.167$ for SDD and 3.217 for LanL2DZ). However, the majority of all the pyramidal boron clusters possess higher dipole moment

and this happens because pyramidal structure shows asymmetric charge distribution but the pristine and bi-pyramidal clusters have inherent symmetric charge distribution.

Ionization Potential and Electron Affinity

The ionization potential (IP) is a key parameter to analyze the stability of the molecular system. Usually IP classify as: Koopmans IP, vertical IP and adiabatic IP. In this study we use Koopmans IP which is the HOMO energies [61]. In our work Koopmans IP are calculated for the lowest energy structures of pristine and inverse-sandwich B_m nanoclusters and presented in Table 5. Among the pristine B_m clusters, B_7 has the largest value of IP. For ZnB_m clusters, ZnB_8 and among the bi-pyramidal clusters, Zn_2B_8 have the largest ionization potential. This all agreeing to the higher stability of these clusters [61].

Hosted file

image7.emf available at <https://authorea.com/users/302041/articles/463473-an-ab-initio-study-on-the-structural-electronic-and-optical-properties-of-inverted-sandwich-monocyclic-small-boron-clusters-znbnm-n-1-2-m-6-8>

Fig. 7 Variations of (a) Ionization Potential (IP) and Electron Affinity (EA) for various B_m clusters by using SDD basis set.

Table 5 Records of ionization potential (IP) and electron affinity (EA) for various pristine and inverted-sandwich boron nanoclusters

System	IP (eV)	IP (eV)	EA (eV)	EA (eV)
	SDD	LanL2DZ	SDD	LanL2DZ
B_6	5.61	5.61	4.84	4.84
ZnB_6	5.67	5.46	3.47	3.35
Zn_2B_6	4.72	4.49	4.63	4.15
B_7	6.63	6.63	4.62	4.62
ZnB_7	5.98	5.94	4.08	3.88
Zn_2B_7	5.46	5.23	4.21	4.17
B_8	5.90	5.90	4.73	4.74
ZnB_8	6.02	6.01	4.87	4.6
Zn_2B_8	6.14	5.95	3.92	3.9

For all the clusters, IP increases for pyramidal system and then decreases for bi-pyramidal system as compared with the pristine system except B_8 clusters. In the B_8 clusters, the value of IP is increased for both the adsorbed clusters as compared to the pristine clusters. The electron affinities (EA) of pristine and Zn adsorbed B_m nanoclusters are also calculated and presented in Table 5. The EA values get decreased for pyramidal clusters and then increased for bi-pyramidal clusters as compared to pristine clusters except all B_7 clusters. This trend is compared with IP and their variations are shown in Fig. 7. The lesser EA value indicates the electronic stability of the clusters and here B_7 , ZnB_6 and Zn_2B_8 are more electronically stable.

Molecular Orbital

The HOMO and LUMO orbital of each system is shown in Fig. 8. Both these orbital are responsible for chemical reaction. Due to having strong covalent bonds, the s and p orbitals of atomic boron are hybridized to produces delocalized, multicentered bonds [73]. For B_6 cluster hybridization and delocalization was orbitals of atomic boron are hybridized to produces delocalized, multicentered bonds [73]. For B_6 cluster hybridization and delocalization was observed. Mostly there are four types of bonds that grasp together the small boron clusters: two-centered σ bonds, three-centered bent σ -type (banana-shaped) bonds, multicentered π -type bonds, and multicentered σ -type bonds [73]. These humble representations get complex with the increase in

s-p hybridization (as the cluster size increases).

Hosted file

image8.emf available at <https://authorea.com/users/302041/articles/463473-an-ab-initio-study-on-the-structural-electronic-and-optical-properties-of-inverted-sandwich-monocyclic-small-boron-clusters-znbnm-n-1-2-m-6-8>

Fig. 8 HOMO-LUMO representation for pristine and inverted sandwich clusters.

Hosted file

image9.emf available at <https://authorea.com/users/302041/articles/463473-an-ab-initio-study-on-the-structural-electronic-and-optical-properties-of-inverted-sandwich-monocyclic-small-boron-clusters-znbnm-n-1-2-m-6-8>

Some more σ -type and π -type bonds are seen for pristine B_7 and B_8 . For pyramidal cluster HOMO is slightly shifted to Zn atom except ZnB_8 where HOMO mainly surrounds the boron ring. On the other hand LUMO's contribution focused on boron atoms. In case of adsorbing two Zn atoms on B_m , an even distribution among all the constituent atoms observed for HOMO whereas LUMO is restricted with the two Zn atoms.

Fig. 9 Density of States (DOS) spectra of pristine and Zn doped (a) B_6 , (b) B_7 and (c) B_8 nanoclusters. Cyan, dark wine and violet color represents the pristine, pyramidal and bi-pyramidal structures respectively.

According to Shuhong Xu et al. the more HOMO-LUMO energy gap is related to the more electron delocalization of the structure [74]. We have observed that the pyramidal B_6 clusters are more delocalized than bi-pyramidal B_6 clusters except in the case of B_8 clusters, bi-pyramidal clusters are more delocalized than pyramidal clusters. While for B_7 clusters, pristine B_7 is more delocalized as compared with the pyramidal and bi-pyramidal clusters

Density of States (DOS) and Energy Gap Analysis

In our study, we have investigated the density of state (DOS) spectra of pristine and adsorbed boron cluster as in Fig. 9, where Fermi level is set to zero. The DOS of a system is the set of numbers of different states at a particular energy level that are allowed to be occupied by electrons and it gives an initial idea about the HOMO-LUMO gap and distribution of unpaired electrons in the system [64]. From Fig. 9, we can predict that impurity states are formed in both HOMO and LUMO region near the Fermi level for adsorbing Zn atom in B_m nanoclusters. More peaks are observed outside the gap region (Fig. 9) when one Zn atom is added and for two Zn atoms Homo spectra almost cross the Fermi level for B_6 cluster and then due to these peaks the E_g values of the ZnB_6 increase and Zn_2B_6 decreases significantly compared to pristine B_6 . For B_7 and B_8 clusters, the peaks of pyramidal clusters are almost coincided with the pristine structures with a slight variation and thus the band gap does not vary that much. But peaks are found in the gap region for Zn_2B_7 which decreases its band gap while for Zn_2B_8 peaks are found outside the gap regions which results large energy gap. The energy gap (E_g) depict the chemical and kinetic stability of the molecule [75]. The HOMO-LUMO energies and the energy gap are listed in Table 4 and the comparisons of HOMO-LUMO gap and their relations with adsorption energy are depicted in Fig. 10.

Hosted file

image10.emf available at <https://authorea.com/users/302041/articles/463473-an-ab-initio-study-on-the-structural-electronic-and-optical-properties-of-inverted-sandwich-monocyclic-small-boron-clusters-znbnm-n-1-2-m-6-8>

Fig. 10 (a) Comparison of bandgap for pristine, pyramidal and bi-pyramidal boron nanoclusters and (b) variations of adsorption energy with energy gap for pyramidal and bi-pyramidal B_m clusters.

For pyramidal B_6 motif, the value of E_g increases from 0.792 eV to 2.198 eV and it decreases to 0.0866 eV for bi-pyramidally adsorbed structure as we already observed in DOS spectra. The exceptionally small E_g value

of Zn_2B_6 has catch interest and we particularly observed the E_g value of Zn_2B_6 for LanL2DZ basis set which is 0.34 eV and it is not very close to SDD value. So, for clarification, more calculations have performed by using some other basis set which are 6-31G (d, p) and 6-311G and tabulated them in Table 6 to compare all the values of E_g for Zn_2B_6 .

Table 6 List of HOMO-LUMO energy gap (in eV unit) by using different basis set for Zn_2B_6 .

Basis Sets	E_{HOMO} (eV)	E_{LUMO} (eV)	E_g (eV)
SDD	-4.720	-4.634	0.086
LanL2DZ	-4.687	-4.150	0.340
6-31G	-4.418	-4.306	0.110
6-311G	-4.639	-4.448	0.191

The calculated E_g values are 0.11eV and 0.191 eV for 6-31G (d, p) and 6-311G basis set respectively and it is quite close to the calculation of SDD basis set. The low band gap of Zn_2B_6 may occurred for the overlying of Zn orbital with boron orbital and this also shows P-type behavior of this cluster. Also, this exceptionally low energy gap indicates electrical conductivity in Zn_2B_6 which cause easy electron transfer. So a transition from semiconducting to metallic phase has occurred for Zn adsorbed B_6 clusters. For B_7 clusters, band gap decreases from pristine cluster to pyramidal and bi-pyramidal clusters which are clearly depicted in Fig. 10 (a) and also in the DOS spectra. Thus for Zn adsorbed B_7 clusters show semiconducting property. For B_8 clusters, energy gap first decreases (ZnB_8) and then increases (Zn_2B_8) and a transition to wide band gap semiconductor occur as the cluster size increases.

Magnetic Properties

Hosted file

image11.emf available at <https://authorea.com/users/302041/articles/463473-an-ab-initio-study-on-the-structural-electronic-and-optical-properties-of-inverted-sandwich-monocyclic-small-boron-clusters-znbnm-n-1-2-m-6-8>

Among all the clusters, pristine and Zn adsorbed B_7 shows magnetism and their spin densities are shown in Fig. 11. As only the pristine B_7 cluster shows dipole moment (0.175) which makes it unique as compared with the other two pristine clusters (B_6 and B_8) and that's why this C_S symmetry of B_7 introduces spin density in the boron framework. For pristine B_7 , the main contribution in spin density comes from B1, B4, B5 and B7 atoms.

Fig. 11 Illustration of Spin density for pristine and Zn adsorbed B_7 nanoclusters (at an iso-value of 0.007 electron/ \AA^3).

After adsorbing one Zn atom, B1, B3, B4, B7 possesses spin density and Zn atom contributes slightly. For bi-pyramidal cluster, the contribution comes from B3, B4, B6 and B7 and also the two Zn atoms contribute slightly to form spin density (Fig. 11). As the boron atoms of the structure mainly contribute to the spin density so they can act as possible active positions for further exohedral functionalization [76].

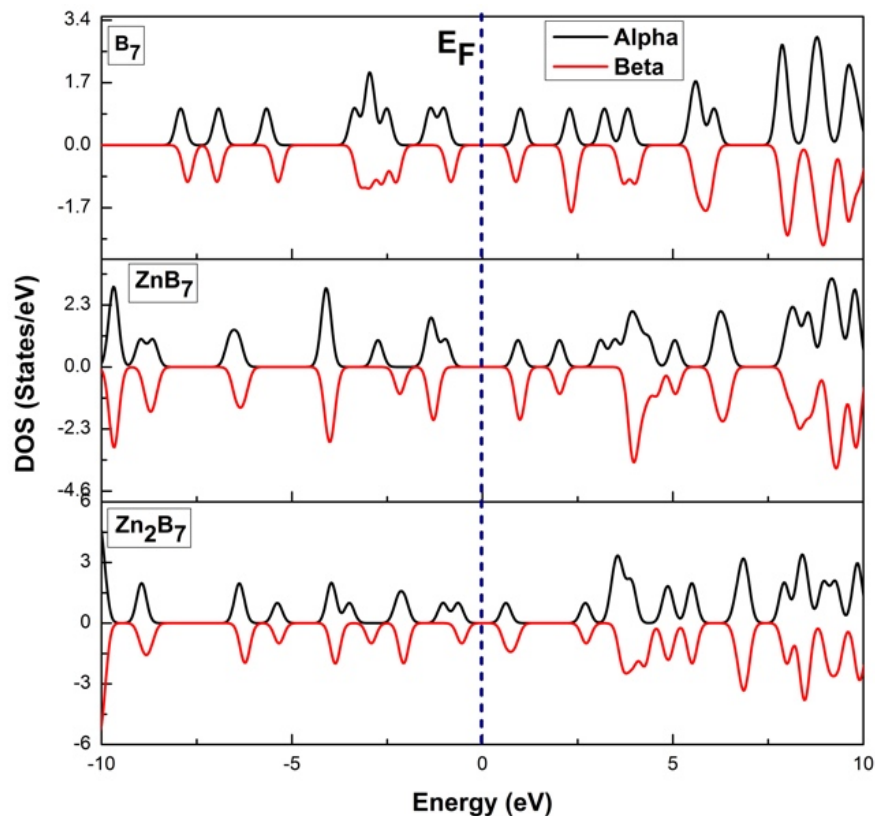


Fig. 12 Alpha and Beta density of states (DOS) spectra of pristine and adsorbed B₇ clusters.

From the dos spectra (Fig. 12), we have observed that the up spin (alpha) and down spin (beta) DOS are not identical and a variation between them is observed for all the clusters. This indicates that these materials induce magnetic properties. So we have calculated their magnetic moments and the value of magnetic moments of B₇, ZnB₇ and Zn₂B₇ are 5.00 μ B, 6.875 μ B and 8.333 μ B respectively. Magnetic moment increases for inverse-sandwich B₇ clusters indicating their transition to strong ferromagnetism.

Optical Properties

Optical property describes the behavior of a material to the photon of light. In this investigation, we have studied Ultraviolet Visible (UV-Vis) spectra and Circular Dichroism (CD) spectra to analyze the optical nature of all the nanoclusters. From UV-Vis spectra, a

(a)	(b)
(c)	(d)

range of wavelength of light is marked that is absorbed for a particular material and is represented by a peak in the graph [77]. The B₆ nanocluster absorbs visible light as evident by the sharp peak at 530 nm and also, a small peak at 340 nm indicates high energy light absorption.

Fig. 13 Graph of Absorption vs wavelength for pristine and adsorbed (a) B₆, (b) B₈ and (c) B₇nanoclusters. (d) Represents the absorption spectra of ZnB₇.

After doping Zn atom, the peak starts to shift left. For ZnB_6 , a peak was found at 330 nm while a wide range peak (200nm-400nm range) was observed for Zn_2B_6 as shown in Fig. 13(a). Pristine B_7 cluster absorbs a wide range of visible light (479nm-595nm). It gives a sharp peak at 947nm which also indicate their potential applications in solar cells [78]. But after adsorption of Zn atom, Zn_2B_7 absorbs a wide range of light (from 363nm to 521 nm) while the absorption peak of ZnB_7 at 1474 nm indicates low energy light absorption. The oscillator strength is found very low for ZnB_7 as compared to pristine B_7 and Zn_2B_7 . That's why in the absorption spectra comparison graph of B_7 clusters, ZnB_7 shows only a straight horizontal line (Fig. 13(c)) and later for better understanding it is depicted individually in Fig. 13(d). B_8 clusters show blue shift after adsorption of Zn atom on the framework (Fig. 13 (b)). Thus, it may conclude that the adsorbed clusters are responsive to high energetic light.

When material absorbs any electromagnetic radiation, then CD spectrum produced for circular polarized light (right and left). It also measures the optical activeness of a material and is mainly found in optically active chiral molecule. In this investigation, we don't have any CD spectrum for all pristine B_m nanoclusters, but we have found CD spectra for the adsorbed clusters as shown in Fig. 14. This reveals the optical activeness of the adsorbed nanoclusters and also shows their chiral effects in nanoscale. Also noticed that CD spectra of these two clusters have different shift and this is because the clusters have different shape and size. Adsorbed nanoclusters possess asymmetric charge distribution and it is one of the crucial reasons they exhibit chirality, and these can be tuned among these clusters.

(a) ZnB_6	(b) Zn_2B_6
(c) ZnB_7	(d) Zn_2B_7
(e) ZnB_8	(f) Zn_2B_8

Fig. 14 CD spectra of Zn adsorbed B_n (n=6-8) nanoclusters.

Chemical Potential and Global Indices

Hosted file

image23.emf available at <https://authorea.com/users/302041/articles/463473-an-ab-initio-study-on-the-structural-electronic-and-optical-properties-of-inverted-sandwich-monocyclic-small-boron-clusters-znbnm-n-1-2-m-6-8>

Chemical potential (μ) and the global indices such as hardness (η), softness (S) and electrophilicity (ω) explain the chemical stability of a structure. HOMO and LUMO energies have been used to calculate them by using equation (8-11) for two basis set and presented in Table 7 and their trend are depicted in Fig. 15. If Chemical potential of a structure decreases, the reactivity of the structure decreases thus the stability increases [79].

Fig. 15 Comparison of (a) hardness (η) and softness (S) (global indices) of all the clusters and variations of chemical potential (μ) and electrophilicity (ω) for (a) B_6 , (b) B_7 and (c) B_8 clusters (pristine, pyramidal and bi-pyramidal) by using SDD basis set.

In this study chemical potentials decrease from pristine B_m to adsorbed (pyramidal and bi-pyramidal) clusters except of ZnB_8 (Fig. 15(c)). This signifies that Zn adsorbed B_m nanoclusters is less reactive than pristine B_m cluster and also stability increases for these adsorbed nanoclusters. On the other hand, it is observed that hardness and softness have built vice-versa relationship and this is depicted in Fig. 15(d). If softness is decreased, then hardness increased which again reaffirms the chemical stability of these nanoclusters.

Table 7 List of Chemical potential (μ) and global indices (Hardness (η), Softness (S) and Electrophilicity (ω)) for two basis set in case of pristine as well as Zn adsorbed B_n nanoclusters (where n= 6-8).

System	Chemical Potential μ (ϵ'')	Chemical Potential μ (ϵ'')	Hardness η (ϵ'')	Hardness η (ϵ'')	Softness S (eV^{-1})	Softness S (eV^{-1})	Electrophilicity ω (ϵ'')	Electrophilicity ω (ϵ'')
	SDD	LanL2DZ	SDD	LanL2DZ	SDD	LanL2DZ	SDD	LanL2DZ
B ₆	-5.225	-5.225	0.385	0.385	1.299	1.299	35.455	35.455
ZnB ₆	-4.570	-4.405	1.100	1.055	0.455	0.474	9.4931	9.196
Zn ₂ B ₆	-4.675	-4.320	0.045	0.170	11.111	2.942	242.840	54.889
B ₇	-5.625	-5.625	1.005	1.005	0.498	0.498	15.742	15.742
ZnB ₇	-5.030	-4.910	0.950	1.030	0.526	0.485	13.316	11.703
Zn ₂ B ₇	-4.835	-4.700	0.625	0.530	0.800	0.944	18.702	20.839
B ₈	-5.315	-5.320	0.585	0.580	0.855	0.862	24.145	24.399
ZnB ₈	-5.445	-5.305	0.575	0.705	0.870	0.709	25.781	19.960
Zn ₂ B ₈	-5.03	-4.925	1.110	1.025	0.450	0.488	11.397	11.832

The electrophilicity first decreased for pyramidal B₆ and then suddenly abruptly increased for bi-pyramidal B₆ clusters as compared to pristine B₆. This sort of opposite case has already been observed for the energy gap value of Zn₂B₆. Here for Zn₂B₆, we have found large value of electrophilicity of 253.581 eV as it shows extremely low HOMO-LUMO gap (0.086 eV). Thus we again performed more investigation with 6-31G and 6-311G basis set for Zn₂B₆ and obtained 169.884 eV and 108.081 eV electrophilicity respectively. As these are close to the value of SDD basis set investigation, so it again endorses our study. The same trend is happen for B₇ clusters but the changes are quite small. For B₈ clusters exception occurred and Zn₂B₈ has low electrophilicity then the pristine and pyramidal clusters as observed in Fig. 15 (c). As electrophilicity is related to chemical stability and an increase in electrophilicity is accompanied by a decrease of chemical stability. So, from our result, we can predict that B₆, ZnB₇ and Zn₂B₈ are chemically more stable than the other clusters.

Conclusions

In this study, we performed comprehensive investigation of the pristine and Zn incorporated inverse-sandwich B_m (n=6-8) nanoclusters at the B3LYP level with two basis sets (SDD and LanL2DZ) in the DFT method. The optimized geometry reveals that all the pristine B_m nanoclusters are in global minimum energy state with point group C_{2h}, C_S and D_{4d} respectively and C₁ for all the adsorbed clusters. The relative stabilities of the adsorbed clusters (according to different calculated parameters) show that Zn₂B_m clusters are more stable among all the adsorbed clusters. Thermodynamic properties imply that chemisorption occurs for all the inverted-sandwich clusters which make them more stable except ZnB₆ and Zn₂B₆ (physisorption occur). Charge distribution analysis signifies that positive charge gets localized on Zn atom and all the boron atoms are negatively charged in the adsorbed nanoclusters except Zn₂B₈ where Zn atom is negatively charged and this is also validated by MEP map. Moreover, pristine B₇ cluster shows spin polarization and all the pyramidal boron clusters possess higher dipole moment because of their asymmetric charge distribution. For that reason, pristine and Zn doped B₇ clusters show magnetism among all the clusters which is witnessed by the spin density and alpha-beta DOS spectra. Magnetic moment increases for adsorbed B₇ clusters indicating their transition to strong ferromagnetism.

According to IP values, pristine B₇, pyramidal ZnB₈ and bi-pyramidal Zn₂B₈ have the largest ionization potential, corresponding to its higher stability. From the molecular orbital, we have observed that pristine B₇, pyramidal B₆ and bi-pyramidal B₈ clusters are more delocalized than the other clusters which indicate their greater stability. In terms of HOMO-LUMO energy gap, inverse-sandwich B_m nanoclusters show semi-conducting property. But exception happened for Zn₂B₆ where we found a transition from semiconducting to metallic phase. By investigating global parameters, we have observed that Zn doped B_m nanoclusters is

less reactive than pristine B_m cluster and Zn_2B_8 are chemically more stable and possesses higher hardness than the other clusters. Absorption spectra shows that Zn adsorbed B_m nanoclusters show blue shift in inverse-sandwich structures and can absorb high energetic light which is very useful for various engineering applications. All the pyramidal and inverse sandwich boron nanoclusters are optically active due to the asymmetric charges in those nanosystems.

Data availability

The data that support our studies are available from the corresponding authors on request.

Funding

We thankfully acknowledge the Higher Education Quality Enhancement Program (HEQEP) subproject CP-3415, University Grant Commission (UGC) of Bangladesh and the World Bank for the financial assistance to set up the Computational Physics (CP) Research Lab in the Department of Physics at Jahangirnagar University. Maliha Nishat is grateful to NST Fellowship under Science and Technology Ministry of Bangladesh for awarding Research Funds.

Ethical declarations

Conflict of interest

The authors declare no conflicts of interest in the current research.

References

1. Castleman AW, Keesee RG (1988) Gas-phase clusters: Spanning the states of matter. *Science* (80-) 241:36–42
2. Becker, EW, Bier, K. & Henkes W (1956) Rays from condensed atoms and molecules in a high vacuum. *J Phys Vol* 146:333–338
3. Romanescu C, Galeev TR, Li WL, et al (2013) Transition-metal-centered monocyclic boron wheel clusters ($M@B_n$): A new class of aromatic borometallic compounds. *Acc Chem Res* 46:350–358
4. Nagamatsu J, Nakagawa N, Muranaka T, et al (2001) Superconductivity at 39 K in magnesium diboride. *Nature* 410:63–64
5. Hussmann B, Pfitzner M (2010) Extended combustion model for single boron particles - Part II: Validation. *Combust Flame* 157:822–833
6. Pan S, Giri S, Chattaraj PK (2012) A computational study on the hydrogen adsorption capacity of various lithium-Doped boron hydrides. *J Comput Chem* 33:425–434
7. Young G, Sullivan K, Zachariah MR, Yu K (2009) Combustion characteristics of boron nanoparticles. *Combust Flame* 156:273–546
8. Grimes RN (2004) Boron Clusters Come of Age. *J Chem Educ* 81:657
9. Boustani I (1997) Systematic ab initio investigation of bare boron clusters: Determination of the geometry and electronic structures of ($n=2-14$). *Phys Rev B - Condens Matter Mater Phys* 55:16426–16438

10. Boustani I (1995) Structure and stability of small boron clusters. A density functional theoretical study. *Chem Phys Lett* 240:135–140
11. Boustani I (1995) A comparative study of ab initio SCF-CI and DFT. Example of small boron clusters. *Chem Phys Lett* 233:273–278
12. Alexandrova AN, Boldyrev AI, Zhai HJ, Wang LS (2006) All-boron aromatic clusters as potential new inorganic ligands and building blocks in chemistry. *Coord Chem Rev* 250:2811–2866
13. Zhai HJ, Kiran B, Li J, Wang LS (2003) Hydrocarbon analogues of boron clusters planarity, aromaticity and antiaromaticity. *Nat Mater* 2:827–833
14. Hanley L, Anderson SL (1987) Production and collision-induced dissociation of small boron cluster ions. *J Phys Chem* 91:5161–5163
15. Zhai HJ, Wang LS, Alexandrova AN, et al (2003) Photoelectron Spectroscopy and ab Initio Study of B3- and B4-Anions and Their Neutrals. *J Phys Chem A* 107:9319–9328
16. Zhai HJ, Wang LS, Alexandrova AN, Boldyrev AI (2002) Electronic structure and chemical bonding of B5- and B5by photoelectron spectroscopy and ab initio calculations. *J Chem Phys* 117:7917–7924
17. Alexandrova AN, Boldyrev AI, Zhai HJ, et al (2003) Structure and bonding in B6- and B6: Planarity and antiaromaticity. *J Phys Chem A* 107:1359–1369
18. Alexandrova AN, Boldyrev AI, Zhai HJ, Wang LS (2004) Electronic Structure, Isomerism, and Chemical Bonding in B7- and B7. *J Phys Chem A* 108:3509–3517
19. Zhai HJ, Alexandrova AN, Birch KA, et al (2003) Hepta- and Octacoordinate Boron in Molecular Wheels of Eight- and Nine-Atom Boron Clusters: Observation and Confirmation. *Angew Chemie - Int Ed* 42:6004–6008
20. Gu FL, Yang X, Tang A, et al (1998) Structure and stability of B+ 13 clusters. *J Comput Chem* 19:203–214
21. Brack M (1993) The physics of simple metal clusters: Self-consistent jellium model and semiclassical approaches. *Rev Mod Phys* 65:677–732
22. Saha P, Rahane AB, Kumar V, Sukumar N (2016) Analysis of the electron density features of small boron clusters and the effects of doping with C, P, Al, Si, and Zn: Magic B7P and B8Si clusters. *Phys Scr* 91:053005
23. Gu J-B, Yang X-D, Wang H-Q, Li H-F (2012) Structural, electronic, and magnetic properties of boron cluster anions doped with aluminum: BnAl - (2[?] n[?] 9). *Chinese Phys B* 21:043102
24. Romanescu C, Galeev TR, Sergeeva AP, et al (2012) Experimental and computational evidence of octa- and nona-coordinated planar iron-doped boron clusters: Fe(c)B8- and Fe(c)B9-. *J Organomet Chem* 721–722:148–154
25. Vijay Kumar, R. V. Beloslouov YK (2006) Alchemy at the nanoscale: Magic heteroatom clusters and assemblies. *ACCMS-2* 36:1–262
26. Yao JG, Wang XW, Wang YX (2008) A theoretical study on structural and electronic properties of Zr-doped B clusters: ZrBn(n = 1–12). *Chem Phys* 351:1–6
27. Li SD, Miao CQ, Guo JC, Ren GM (2006) Transition metal-boron complexes BnM: From bowls (n = 8–14) to tires (n = 14). *J Comput Chem* 27:1858–1865
28. Liu X, Zhao G, Guo L, et al (2007) Structural, electronic, and magnetic properties of MBn (M=Cr,Mn,Fe,Co, Ni, nI7) clusters. *Phys Rev A* 75:063201

29. Ito K, Pu Z, Li QS, Schleyer PVR (2008) Cyclic boron clusters enclosing planar hypercoordinate cobalt, iron, and nickel. *Inorg Chem* 47:10906–10910
30. Galeev TR, Romanescu C, Li WL, et al (2012) Observation of the highest coordination number in planar species: Decacoordinated Ta(c)B10- and Nb(c)B10-anions. *Angew Chemie - Int Ed* 51:2101–2105
31. Romanescu C, Galeev TR, Li WL, et al (2013) Geometric and electronic factors in the rational design of transition-metal-centered boron molecular wheels. *J Chem Phys* 138:134315
32. Xu C, Cheng L, Yang J (2014) Double aromaticity in transition metal centered double-ring boron clusters $M@B_2n$ ($M = Ti, Cr, Fe, Ni, Zn; N = 6, 7, 8$). *J Chem Phys* 141:124301
33. Rakib Hossain M, Milon, Hasan SM, et al (2018) The planar B6 cluster as a motif for doping metal cation (Al³⁺): A DFT study. 2nd Int Conf Electr Electron Eng ICEEE 2017 1–4
34. Rakib Hossain M, Milon, Hasan SM, et al (2018) Structural, Electronic and Optical Properties of Pristine and Metal Doped B6 Nanocluster: A DFT Study. 5th IEEE Reg 10 Humanit Technol Conf 2017 (R10-HTC 2017) 2018-Janua:209–212
35. Milon, Hasan SM, Md Hossain R, et al (2018) Investigation of Semiconductor Doped B6 Nanocluster: A First Principle Study. 2nd Int Conf Electr Electron Eng ICEEE 2017 1342:1–4
36. Hasan SM, Milon, Hossain MR, et al (2018) Hexagonal boron cluster as an anode material for divalent-ion (Ca²⁺) storage: A theoretical study. 5th IEEE Reg 10 Humanit Technol Conf 2017 (R10-HTC 2017) 242–245
37. Li W-L, Xie L, Jian T, et al (2014) Hexagonal Bipyramidal [Ta₂B₆]⁰ Clusters: B₆ Rings as Structural Motifs. *Angew Chemie Int Ed* 53:1288–1292
38. Shinde R, Shukla A (2012) Large-Scale First Principles Configuration Interaction Calculations of Optical Absorption in Boron Clusters. *Nano Life* 02:1240004
39. Li W, Chen T, Xing D, et al (2018) Observation of highly stable and symmetric lanthanide octa-boron inverse sandwich complexes. *PNAS* July 24 115:E6972–E6977
40. Kriek S, Go H, Yu L, et al (2009) Stable “Inverse” Sandwich Complex with Unprecedented Organocalcium(I): Crystal Structures of [(thf)₂Mg(Br)-C₆H₂-2,4,6-Ph₃] and [(thf)₃Ca{μ-C₆H₃-1,3,5-Ph₃}Ca(thf)₃] Sven. *J Am Chem Soc* 131:2977–2985
41. Nishat M, Hossain MR, Israt MF, et al (2019) First principle study of pristine and Zn doped B6 nanocluster. In: 2019 International Conference on Sustainable Technologies for Industry 4.0, STI 2019. IEEE, pp 1–5
42. Xu Q, Cai W, Zhang M, et al (2018) Photoluminescence mechanism and applications of Zn-doped carbon dots. *RSC Adv* 8:17254–17262
43. Shen L, Dadras J, Alexandrova AN (2014) Pure and Zn-doped Pt clusters go flat and upright on MgO(100). *Phys Chem Chem Phys* 16:26436–26442
44. Pal M, Lee S, Kwon D, et al (2017) Direct immobilization of antibodies on Zn-doped Fe₃O₄ nanoclusters for detection of pathogenic bacteria. *Anal Chim Acta* 952:81–87
45. Becke AD (1993) A new mixing of Hartree-Fock and local density-functional theories. *J Chem Phys*
46. Lee C, Yang W, Parr RG (1988) Development of the Colle-Salvetti correlation-energy formula into a functional of the electron density. *Phys Rev B*
47. M. J. Frisch, G. W. Trucks, H. B. Schlegel, G. E. Scuseria, M. A. Robb, J. R. Cheeseman, G. Scalmani, V. Barone, G. A. Petersson, H. Nakatsuji, X. Li, M. Caricato, A. V. Marenich, J. Bloino, B. G. Janesko, R. Gomperts, B. Mennucci, H. P. Hratchian J V. (2016) Gaussian 16, (Revision B.01)

48. Wadt WR, Hay PJ (1985) Ab initio effective core potentials for molecular calculations. Potentials for main group elements Na to Bi. *J Chem Phys* 82:284–298
49. Cao X, Dolg M (2004) Segmented contraction scheme for small-core actinide pseudopotential basis sets. *J Mol Struct THEOCHEM*. <https://doi.org/10.1016/j.theochem.2003.12.015>
50. Rad AS, Nasimi N, Jafari M, et al (2015) Ab-initio study of interaction of some atmospheric gases (SO₂, NH₃, H₂O, CO, CH₄ and CO₂) with polypyrrole (3PPy) gas sensor: DFT calculations. *Sensors Actuators, B Chem* 220:641–656
51. Shokuhi Rad A, Zardoost MR, Abedini E (2015) First-principles study of terpyrrole as a potential hydrogen cyanide sensor: DFT calculations. *J Mol Model* 21:273
52. Chen L, Xu C, Zhang XF, Zhou T (2009) Raman and infrared-active modes in MgO nanotubes. *Phys E Low-Dimensional Syst Nanostructures* 41:852–855
53. Rani P, Jindal VK (2013) Designing band gap of graphene by B and N dopant atoms. *RSC Adv* 3:802–812
54. Zou M, Zhang J, Chen J, Li X (2012) Simulating adsorption of organic pollutants on finite (8,0) single-walled carbon nanotubes in water. *Environ Sci Technol* 46:8887–8894
55. Bandyopadhyay D (2012) Chemisorptions effect of oxygen on the geometries, electronic and magnetic properties of small size Ni_n(n = 1-6) clusters. *J Mol Model* 18:737–749
56. Rezaei-Sameti M, Yaghoobi S (2015) Theoretical study of adsorption of CO gas on pristine and AsGadoped (4, 4) armchair models of BPNTs. *Comput Condens Matter* 3:21–29
57. Rezaei-Sameti M (2012) The effect of doping three Al and N atoms on the chemical shielding tensor parameters of the boron phosphide nanotubes: A DFT study. *Phys B Condens Matter* 407:22–26
58. Kato H, Tanaka E (1991) Stabilities of small Benand Bnclusters (4 [?] n [?] 8) by vibrational analysis. *J Comput Chem* 12:1097–1109
59. Li QS, Jin Q, Luo Q, et al (2003) Structure and stability of B₆, B₆⁺, and B₆⁻ clusters. *Int J Quantum Chem* 94:269–278
60. Ma J, Li Z, Fan K, Zhou M (2003) Density functional theory study of the B₆, B₆⁺, B₆⁻, and B₆²⁻ clusters. *Chem Phys Lett* 372:708–716
61. Feng XJ, Luo YH (2007) Structure and stability of Al-doped boron clusters by the density-functional theory. *J Phys Chem A* 111:2420–2425
62. Li QS, Gong LF, Gao ZM (2004) Structures and stabilities of B₇, B₇⁺ and B₇⁻ clusters. *Chem Phys Lett* 390:220–227
63. Baxter R, Hastings N, Law A, Glass EJ (2008) A rapid and robust sequence-based genotyping method for BoLA-DRB3 alleles in large numbers of heterozygous cattle. *Short Commun* 39:561–563
64. Rad AS, Shabestari SS, Jafari SA, et al (2016) N-doped graphene as a nanostructure adsorbent for carbon monoxide: DFT calculations. *Mol Phys* 114:1756–1762
65. Jaque P, Toro-Labbé A (2002) Characterization of copper clusters through the use of density functional theory reactivity descriptors. *J Chem Phys* 117:3208–3218
66. Varghese S, Swaminathan S, Singh K, Mittal V (2016) Energetic Stabilities, Structural and Electronic Properties of Monolayer Graphene Doped with Boron and Nitrogen Atoms. *Electronics* 5:91
67. Özer A, Özer D, Özer A (2004) The adsorption of copper(II) ions on to dehydrated wheat bran (DWB): Determination of the equilibrium and thermodynamic parameters. *Process Biochem* 39:2183–2191

68. Krishnakumar V, Barathi D, Mathammal R, et al (2014) Spectroscopic properties, NLO, HOMO-LUMO and NBO of maltol. *Spectrochim Acta - Part A Mol Biomol Spectrosc* 121:245–253
69. Bulat FA, Toro-Labbé A, Brinck T, et al (2010) Quantitative analysis of molecular surfaces: Areas, volumes, electrostatic potentials and average local ionization energies. *Mol Model* 16:1679–91
70. Bulat FA, Burgess JS, Matis BR, et al (2012) Hydrogenation and fluorination of graphene models: Analysis via the average local ionization energy. *J Phys Chem A* 116:8644–8652
71. Rad AS, Valipour P, Gholizade A, Mousavinezhad SE (2015) Interaction of SO₂ and SO₃ on terthiophene (as a model of polythiophene gas sensor): DFT calculations. *Chem Phys Lett* 639:29–35
72. Loukhovitski BI, Sharipov AS, Starik AM (2017) Quantum chemical study of small Al_nB_mclusters: Structure and physical properties. *Chem Phys* 493:61–76
73. Luke Hanely JLW and SLA (1988) Collision- Induced Dissociation and ab Initio Studies of Boron Cluster Ions: Determination. *Phys Chem* 92:5803–5812
74. Xu S, Dong R, Lv C, et al (2017) Configurations and characteristics of boron and B₃₆clusters. *Mol Model* 23:198
75. Harwood LM, Moody CJ, Percy JM (1998) Experimental organic chemistry : standard and microscale. *Exp Org Chem Stand microscale* 2nd:127–132
76. Jin P, Hou Q, Tang C, Chen Z (2015) Computational investigation on the endohedral borofullerenes M@B₄₀(M = Sc, Y, La). *Theor Chem Acc* 134
77. Hay PJ, Wadt WR (1985) Ab initio effective core potentials for molecular calculations. Potentials for K to Au including the outermost core orbitale. *J Chem Phys* 82:299–310
78. Sarkar S, Bhattacharjee K, Das GC, Chattopadhyay KK (2014) Self-sacrificial template directed hydrothermal route to kesterite-Cu₂ZnSnS₄ microspheres and study of their photo response properties. *CrystEngComm* 16:2634
79. Job G, Herrmann F (2006) Chemical potential - A quantity in search of recognition. *Eur J Phys* 27:353–371

Hosted file

journal table.docx available at <https://authorea.com/users/302041/articles/463473-an-ab-initio-study-on-the-structural-electronic-and-optical-properties-of-inverted-sandwich-monocyclic-small-boron-clusters-znbnm-n-1-2-m-6-8>